Available online at www.sciencedirect.com
SCIENCE DIRECT®
International Journal of Heat and Fluid Flow 24 (2003) 41–53
International Journal of HEAT AND FLUID FLOW
www.elsevier.com/locate/ijhff

Instability in a rotating channel–cavity system with an axial through-flow

Isabelle Raspo [a,*], Emilia Crespo del Arco [b]

[a] M.S.N.M., F.R.E. 2405/C.N.R.S., I.M.T.-La Jetée, Technopôle de Château-Gombert, 38 rue Frédéric Joliot Curie, 13451 Marseille Cedex 20, France
[b] U.N.E.D., Dpto. Fisica Fundamental, Apdo. 60141, 28080 Madrid, Spain

Received 3 December 2000; accepted 15 June 2002

Abstract

This paper is devoted to the numerical study of time-dependent flows that develop in a Taylor–Couette-like configuration (the outer cylinder exhibiting a side cavity) with a superposed axial through-flow, which is relevant to turbomachinery applications. Depending on the differential rotation rate between the inner cylinder and the cavity walls, the base flow can be either convectively or absolutely unstable, and then wave packets consisting of several small toroidal vortices appear near the inner cylinder and travel downstream. The influence of the different control parameters and of the inlet condition on the occurence of the patterns is analyzed. The flow simulations were obtained by using a spectral approximation coupled with a domain decomposition method for the solution of the axisymmetric time-dependent Navier–Stokes equations in the vorticity–streamfunction formulation.

Keywords: Taylor–Couette-like configuration; Convective instability; Absolute instability; Spectral approximation; Domain decomposition technique

1. Introduction

In the present study, we report numerical solutions of the flow in a Taylor–Couette configuration when an axial flow is superimposed and when the basic geometry is complicated by the presence of a side cavity, as represented in Fig. 1. This configuration is relevant for the study of aircooling systems in rotating machines and models the space between two high pressure compressor discs in a gas turbines engine. Air is introduced in order to cool the compressor discs and then the turbine discs which are located downstream of the combustion chamber. As a consequence, the values of the control parameters (Reynolds and Taylor numbers) are higher than those found elsewhere in the literature for open Taylor–Couette flows.

The hydrodynamic stability of Taylor–Couette flow between concentric rotating cylinders has been extensively studied theoretically and the stability regions have been confirmed by experiments (Chandrasekhar, 1961). The base flow, which is a simple solution of the Navier–Stokes equations, consists of steady axisymmetric cylindrical streamtubes. When the Taylor number exceeds a critical value, the flow becomes unstable giving rise to the well known axisymmetric Taylor vortices (TV). The stability of the Taylor–Couette flow for a gap of arbitrary radius ratio was investigated by Sparrow et al. (1964) who showed that the critical Taylor number depends strongly on the radius ratio. More precisely, the smaller the radius ratio is, the larger the critical Taylor number is. When an axial flow is superposed, the results of the stability analysis of viscous flow showed that the threshold for the Taylor instability is delayed for increasing values of the Reynolds number (Chandrasekhar, 1961). In the open configuration, the instability is oscillatory in time and leads to propagating Taylor vortices (PTV) that drift in the direction of the flow at a velocity proportional to the flow velocity. Moreover, the first instability is convective.

The determination of the thresholds for convective and absolute instability in a Taylor–Couette system with an axial through-flow and the investigation of the PTV's

* Corresponding author. Tel.: +33-4-91-11-85-49; fax: +33-4-91-11-85-02.
E-mail address: isabel@13m.univ-mrs.fr (I. Raspo).

0142-727X/02/$ - see front matter © 2002 Elsevier Science Inc. All rights reserved.
PII: S0142-727X(02)00193-5

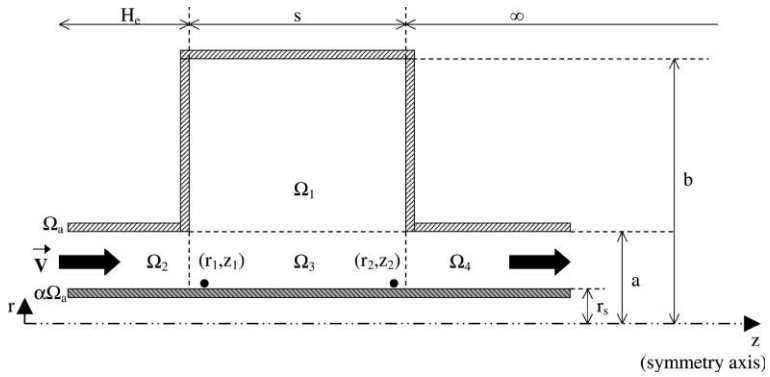

Fig. 1. Geometry.

characteristics in each unstable region have been the subject of several theoretical and experimental works in the past decade (Babcock et al., 1992, 1994; Tsameret and Steinberg, 1994a; Tsameret et al., 1994; Büchel et al., 1996). These studies showed in particular that, for a fixed value of the forced flow, there exist two values of the inner cylinder rotation rate for the onset of instabilities. First, the transition to convective instability occurs for a critical value of the rotation rate slightly greater than the one for the Taylor instability (i.e. in the configuration without through-flow). Then, by increasing the inner cylinder rotation rate, a second onset, corresponding to the transition to absolute instability, is reached. The two critical values of the rotation rate increase with increasing Reynolds number. Moreover, the PTV sustained in the convectively unstable region were found to be noise-sustained structures generated by a process of permanent noise amplification (Tsameret et al., 1994). The base flow amplifies the microscopic noise leading to macroscopic travelling patterns. Babcock et al. (1992) estimated the strength of the noise which drives the PTV. Comparing their experimental measurements with numerical simulations of the stochastic Ginsburg–Landau equation, they concluded that the noise-sustained structures in the convectively unstable regime are the result of thermal noise amplification. The more recent study of Tsameret et al. (1994) suggested that there are two different sources of noise in open Taylor–Couette systems. For small values of the forced flow, the intensity of the intrinsic noise is saturated at a constant noise level independent of the Reynolds number and close to the estimated thermal noise level. On the other hand, for large values of the forced flow, it drastically increases with the Reynolds number, leading to the conclusion that the perturbations of the flow at the inlet boundary are the most important source of noise in this case.

In the absolutely unstable regime, the structural dynamics of pattern formation substantially differ from that observed in the convectively unstable one. The absolute instability is governed by non-linear contributions in the balance equations. Büchel et al. (1996) studied the spatiotemporal characteristics of the PTV associated with the absolute instability by solving numerically the axisymmetric incompressible Navier–Stokes equations and the 1D Ginzburg–Landau amplitude equation. Their results showed that, in the absolutely unstable region, the patterns, which are uniquely selected, are independent of parameter history, initial conditions and system length. On the other hand, they depend on the inlet and outlet boundary conditions, in addition to the inner cylinder rotation rate and to the Reynolds number. Büchel et al. (1996) showed also that this pattern selection can be described by a non-linear eigenvalue problem with the frequency as eigenvalue.

The structures and the dynamics of the PTV have been studied experimentally by Werely and Lueptow (1999) by using particle image velocimetry for a relatively large range of parameters. In addition to PTV, the experiments of Tsameret and Steinberg (1994b) revealed the existence of other pattern states in Taylor–Couette systems with an axial through-flow, such as stationary spirals and moving spirals and more complex states resulting from the competition between the three basic modes. However, the phase diagram that they established suggests that, except for a region of intermediate values of the Reynolds number, the first mode observed when increasing the inner cylinder rotation rate is the PTV mode.

In our system, the basic Taylor–Couette configuration is complicated by the presence of the side cavity. Moreover, in addition to the rotation of the inner cylinder, the system is also submitted to the rotation of the cavity and the channel outer walls, unlike the configuration investigated in the major part of experiments. The numerical solutions of this problem revealed that, in the unstable regime, small vortices travel downstream near the inner cylinder. These vortices exhibit several spatiotemporal characteristics of the PTV observed experimentally in the classical open Taylor–Couette system. When the base flow is convectively unstable, the noise induced by the inlet boundary condition in our problem

is sufficient to sustain the structures since the Reynolds numbers that we considered are much larger than the range investigated in previous works. The entry length necessary for the flow to get rid of the inlet perturbation was theoretically estimated and it was found to be proportional to the Reynolds number. Moreover, the perturbation due to the inlet condition, which was also theoretically estimated, was found to increase strongly with the entry length.

The first section is devoted to the description of the physical problem and the mathematical modelling. The numerical method based on a spectral approximation and on a domain decomposition technique is also introduced. In the second section, we first establish the existence of an entry zone due to the inlet boundary condition for the azimuthal velocity. Then, the results concerning PTV at low Reynolds numbers and convective and absolute instability at high Reynolds numbers are discussed. In the final section, some results obtained in the classical Taylor–Couette system (i.e. without the side cavity) corroborate the conclusions of the previous section.

2. Mathematical formulation and numerical method

2.1. Physical problem and mathematical modelling

The physical model consists of an annular channel of inner radius r_s and outer radius a, which exhibits on a part of its outer wall a side cavity ($a \leqslant r \leqslant b$, with b the outer radius of the cavity) located at $H_e \leqslant z \leqslant H_e + s$ (with s the width of the cavity) from the channel inlet $z = 0$ (Fig. 1). The outer cylinder and the cavity walls rotate around the axis ($0z$) with the angular velocity Ω_a. The inner cylinder, called the central shaft, rotates faster, with an angular velocity $\alpha\Omega_a$ (with $\alpha \geqslant 1$). The flow enters at the annular channel inlet and leaves the cavity through the extension of the channel which is semi-infinite ($H_e + s \leqslant z < +\infty$, $r_s \leqslant r \leqslant a$).

The variables are made dimensionless by taking as characteristic scales b for lengths, $\Omega_a b$ for velocities and $1/\Omega_a$ for time. Then, the physical parameters are the Ekman number $E = \nu/(\Omega_a b^2)$, with ν the kinematic viscosity, and the Reynolds number $Re_z = 2(a - r_s)V_0/\nu$ which characterizes the forced flow, with V_0 the axial velocity maximum at the channel inlet. The parameter characterizing the non-linearity of the flow is the Rossby number $Ro = 2V_0/(3\Omega_a a)$. The geometry of the system is defined by two gap ratios, $G_1 = H_e/b$ and $G_2 = s/b$, and two radius ratios, $\gamma_1 = r_s/b$ and $\gamma_2 = a/b$.

We consider time-dependent, axisymmetric and incompressible flows. The governing equations are therefore the axisymmetric Navier–Stokes equations which are considered here in the vorticity ω–streamfunction ψ formulation. In a relative frame rotating with the angular velocity Ω_a, the dimensionless equations are

$$\frac{\partial\omega}{\partial t} + u\frac{\partial\omega}{\partial r} + w\frac{\partial\omega}{\partial z} - \frac{u\omega}{r} = E\left(\Delta\omega - \frac{\omega}{r^2}\right) + 2\frac{v}{r}\frac{\partial v}{\partial z} + 2\frac{\partial v}{\partial z} \tag{1}$$

$$\frac{\partial v}{\partial t} + u\frac{\partial v}{\partial r} + w\frac{\partial v}{\partial z} + \frac{uv}{r} = E\left(\Delta v - \frac{v}{r^2}\right) - 2u \tag{2}$$

$$\Delta'\psi - \omega r = 0 \tag{3}$$

where Δ and Δ' are the Laplacian operators expressed in cylindrical coordinates and defined by

$$\Delta = \frac{\partial^2}{\partial r^2} + \frac{1}{r}\frac{\partial}{\partial r} + \frac{\partial^2}{\partial z^2}$$

$$\Delta' = \frac{\partial^2}{\partial r^2} - \frac{1}{r}\frac{\partial}{\partial r} + \frac{\partial^2}{\partial z^2}$$

and u, v and w are respectively the radial, azimuthal and axial components of velocity in the relative frame. The vorticity ω and the streamfunction ψ are defined from the velocity components by the formulas:

$$\omega = \frac{\partial u}{\partial z} - \frac{\partial w}{\partial r} \quad \text{and} \quad u = \frac{1}{r}\frac{\partial\psi}{\partial z}, \quad w = -\frac{1}{r}\frac{\partial\psi}{\partial r}$$

No-slip conditions are prescribed on the channel and cavity walls. At the channel inlet, a parallel axial flow is imposed: the radial velocity u is set equal to zero, a parabolic profile with a maximum equal to V_0 is prescribed for the axial velocity, and the fluid rotates at the same angular velocity as the outer channel wall. The channel being semi-infinite, fully developed flow conditions are assumed at outlet. These conditions are chosen in order to not disturb the upstream flow. The above boundary conditions can be written for the vorticity–streamfunction formulation as

$$\psi = 0, \quad \frac{\partial\psi}{\partial n} = 0, \quad v = 0 \quad \text{for} \begin{cases} r = \gamma_2 \text{ and } 0 \leqslant z \leqslant G_1 \\ r = \gamma_2 \text{ and } G_1 + G_2 \leqslant z < +\infty \\ r = 1 \text{ and } G_1 \leqslant z \leqslant G_1 + G_2 \\ z = G_1 \text{ or } z = G_1 + G_2 \text{ and } \gamma_2 \leqslant r \leqslant 1 \end{cases} \tag{4}$$

where $\partial/\partial n$ denotes the normal derivative.

$$\psi(\gamma_1, z, t) = \frac{\gamma_1 + \gamma_2}{6} Re_z E, \quad \frac{\partial\psi}{\partial r}(\gamma_1, z, t) = 0,$$
$$v(\gamma_1, z, t) = (\alpha - 1)\gamma_1 \qquad \text{for } 0 \leqslant z < +\infty \tag{5}$$

$$\psi(r, 0, t) = \frac{2}{(\gamma_2 - \gamma_1)^3} Re_z E\left[\frac{r^4}{4} - (\gamma_2 + \gamma_1)\frac{r^3}{3} + \frac{\gamma_1\gamma_2}{2}r^2 + \frac{\gamma_2^3(\gamma_2 - 2\gamma_1)}{12}\right]$$

$$\frac{\partial\psi}{\partial z}(r, 0, t) = 0, \quad v(r, 0, t) = 0 \qquad \text{for } \gamma_1 \leqslant r \leqslant \gamma_2 \tag{6}$$

$$\frac{\partial\omega}{\partial z}(r,z,t)=0,\quad \frac{\partial\psi}{\partial z}(r,z,t)=0,\quad \frac{\partial v}{\partial z}(r,z,t)=0 \quad \text{for } \gamma_1\leqslant r\leqslant\gamma_2 \text{ and } z\to+\infty \tag{7}$$

2.2. Numerical method

The Eqs. (1)–(3) with the boundary conditions (4)–(7) are solved using a domain decomposition method coupled with a pseudo-spectral approximation (Raspo et al., 1996; Raspo, 1996; Raspo, in press). The time integration is performed through a second order backward Euler scheme with a fully implicit discretization of the diffusive terms and an Adams–Bashforth evaluation of the convective terms. The resulting set of equations, consisting of a Stokes problem for (ω,ψ) and a Helmholtz problem for the azimuthal velocity v, is then solved using a collocation Chebyshev approximation in both r and z space directions. Hence, coordinate transformations are performed in each subdomain Ω_i to change it into the square domain $[-1,+1]\times[-1,+1]$ in which the Chebyshev polynomials are defined. For the semi-infinite outlet subdomain, the coordinate transformation in the axial direction must change it into a finite domain and also concentrate the calculation points near the subdomain inlet, in order to ensure a satisfactory accuracy in the downstream region. These constraints are satisfied by using the coordinate transformation defined by

$$Z=\alpha\tanh(z/2)+\beta \quad \text{for } G_1+G_2\leqslant z\leqslant+\infty \quad \text{with}$$

$$\alpha=\frac{2}{1-\tanh((G_1+G_2)/2)} \quad \text{and}$$

$$\beta=-\frac{1+\tanh((G_1+G_2)/2)}{1-\tanh((G_1+G_2)/2)}$$

Then, the solution (ω,ψ,v) is approximated locally in each subdomain Ω_i by Chebyshev polynomials of degree at most equal to N_i in the r-direction and to M_i in the z-direction. The approximation $\varphi_{N_iM_i}$, for $\varphi=\omega,\psi,v$, is computed at each couple of points (Y_n,Z_m) in Ω_i, with Y_n, $n=0,\ldots,N_i$, and Z_m, $m=0,\ldots,M_i$, the Gauss–Lobatto collocation points. Finally, all the resulting Helmholtz type problems are solved using a full matrix diagonalization technique.

The semi-complex geometric configuration of the system, with a T-shape, cannot be treated with a monodomain spectral method. So the computational domain is divided into four rectangular subdomains, with one subdomain corresponding to the side cavity (subdomain Ω_1) and the other three subdomains (Ω_2, Ω_3 and Ω_4) corresponding to the channel (Fig. 1). The continuity conditions at the interface between adjacent subdomains, which assess the continuity of the variables and of their first order normal derivative, are prescribed through the influence matrix technique (Vanel et al., 1986), which is used also to solve the Stokes problem coupling the vorticity and the streamfunction in each subdomain. This approach allows one to obtain directly, by simply inverting the continuity matrix, the values of the variables at the interface. The detailed description and the study of this multidomain method can be found in Raspo et al. (1996), Raspo (1996, in press) . It should be noted that the domain decomposition is also efficient to solve the vorticity singularities existing at the two re-entrant corners (upstream and downstream corners of the cavity) by isolating them at subdomains corners. Hence, the negative effects of the singularities on the computed solution (loss of accuracy, Gibbs oscillations) can be significantly reduced, allowing a satisfactory accuracy to be obtained (Raspo, 1996, in press). On the other hand, the very high vorticity gradients in the zones surrounding the re-entrant corners are, of course, taken into account in the computation.

The results presented in next sections were obtained for gap ratios $G_1=0.24$ and $G_2=1.36$ and radius ratios $\gamma_1=0.08$ and $\gamma_2=0.32$, with a resolution $N_1\times M_1=40\times80$ and $N_i\times M_i=30\times80$ for $i=2,3,4$. The time-step used is $\delta t=10^{-4}$ for all the computations. It should be noted that, in all the figures, only a finite part of the semi-infinite outlet subdomain is drawn.

Finally, we have verified that the instability phenomena observed are not due to a lack of numerical accuracy and persist when the resolution is increased. Indeed, for $Re_z=196$, $E=5\times10^{-4}$ and $\alpha=14$, the same instability phenomenon was obtained for the resolution $N_1\times M_1=40\times80$ and $N_i\times M_i=30\times80$ for $i=2,3,4$ and for an increased resolution $N_1\times M_1=54\times90$ and $N_i\times M_i=40\times90$ for $i=2,3,4$ (Raspo, 1996). Moreover, the difference on the maximum of the streamfunction disturbances (maximum value which is obtained at the position of the small vortices) is about 5%.

3. Results

In their investigation on instabilities in a Taylor–Couette system with an axial through-flow, Babcock et al. (1992, 1994), Tsameret and Steinberg (1994a,b) and Tsameret et al. (1994) used as relevant parameter, in addition to the Reynolds number, the reduced rotation speed of the inner cylinder $\varepsilon=\Omega/\Omega_c-1$ (where Ω is the rotation of the inner cylinder and Ω_c refers to the onset of TV in the case without through-flow). However, the use of this parameter requires the knowledge of the value of Ω_c. That is why we chose to use as control parameter the Taylor number instead of ε, although this latter parameter seems to be more appropriate for the study of instabilities in open Taylor–Couette systems. Chandrasekhar (1961) defines the Taylor number by

$$Ta = \frac{1}{2}(1+\alpha^{-1})\left(\frac{2\alpha\Omega_a a^2}{\nu}\right)^2 \frac{(1-\eta)^3(\eta^2-\alpha^{-1})}{(1+\eta)}$$

with η the radius ratio: $\eta = r_s/a = \gamma_1/\gamma_2$.

For a given value of η and α, instability will set in for a certain critical value Ta_c of the Taylor number. This critical value has been determined theoretically for several values of the radius ratio η in a Taylor–Couette configuration (i.e. without through-flow) by Sparrow et al. (1964) and for narrow gaps in the presence of an axial forced flow by Chandrasekhar (1961). Their results are presented in Table 1, in which the characteristics of the flow (wave number k_c, frequency f_c and phase velocity V_ϕ) at the critical conditions are also reported. It must be noted that the frequencies are made dimensionless by taking a characteristic frequency as $\nu/(a-r_s)^2$.

In the case of the classical Taylor–Couette configuration, the studies of Sparrow et al. revealed that the critical Taylor number depends strongly on the values of α and η. More precisely, Ta_c increases with α and, on the other hand, the smaller η is, the larger Ta_c is. They showed also that the wave number at which the onset of instability occurs behaves similarly. On the other hand, Chandrasekhar observed that the critical Taylor number, together with the instability wave number, the frequency and the phase velocity, increase with the Reynolds number.

The parameters for the various cases that we have treated are listed in Table 2. When the flow is unstable, the instability wave number k, frequency f and phase velocity V_ϕ are reported. It must be noted that the frequency f refers to that of the solution in the channel below the upstream part of the cavity. That is why no frequency is reported in the case of convective instability, since the flow becomes stationary in this part of the system. On the other hand, when the flow is quasi-periodic, the two uncommensurable frequencies are given in the table.

3.1. Estimation of the entry length

The flow enters the channel with the rotation speed of the outer wall, $\Omega_a r$. This inlet condition induces a perturbation of the azimuthal velocity at inlet near the inner cylinder, since this velocity component is equal to $\alpha\Omega_a r_s$ on the central shaft. Therefore, the perturbation due to the inlet condition, which is the most important source of noise for large Reynolds numbers (Tsameret et al., 1994), increases with α. The flow then requires some streamwise distance, termed here entry length, to recover the azimuthal velocity of the base flow. In the

Table 1
Critical values of the TV and of the PTV given by Sparrow et al. (1964) and Chandrasekhar (1961)

	η	α	Ta_c	k_c	f_c	Re_z	V_ϕ/V_0	
Sparrow et al. (1964)	0.95	∞	1755	$\sim\pi$	0	0	0	TV
	0.25	∞	7442	3.24				TV
	0.25	21.3	5961	3.225				TV
	0.25	16.7	5660	3.210				TV
Chandrasekhar (1961)	$\to 1$	∞	1715	3.14	0	0	0	TV
			1753	3.1	12.6	15	0.542	PTV
			5962	5.2	270.2	180	0.577	PTV
			8319	6.0	425	240	0.590	PTV

Table 2
Present results

	η	α	Ta	k	f	Re_z	V_ϕ/V_0	
Channel–cavity system	0.25	14	−53,084			10		Stable
		16.5	15,483	5.87	34.5	10	0.86	PTV
		8	−127,402			196		Stable
		14	−53,084	9.19		196	1	CU
		17.5	49,103	9.73	25, 167	196	1	AU
		17.5	49,103	9.37	199	300	0.84	AU
		17.5	49,103	8.72	294	500	0.41	AU
		17.5	49,103	8.24		650	0.25	CU
		17.5	49,103	7.18		800	0.22	CU
		17.5	12,276	8.47		196	0.61	CU
Taylor–Couette system	0.25	14	−53,084	10.18		196	0.97	CU
		17.5	49,103	10.14	29, 159	196	0.97	AU

CU: convectively unstable flow, AU: absolutely unstable flow, PTV: propagating Taylor vortices.

following, we establish a theoretical estimation of this entry length and of the inlet perturbation of azimuthal velocity.

The rotating flow is in equilibrium when the centrifugal force, $\rho v^2/r$ with ρ the density, is balanced by a radial pressure gradient. Therefore, the base flow exhibits a radial velocity $u_0(r) = 0$ and an azimuthal velocity $v_0(r)$ which satisfies the equation

$$\left(\frac{\partial^2 v_0}{\partial r^2} + \frac{1}{r}\frac{\partial v_0}{\partial r} - \frac{v_0}{r^2}\right) = 0$$

with the boundary conditions:

$$v_0(\gamma_1) = \alpha\gamma_1$$
$$v_0(\gamma_2) = \gamma_2$$

The dimensionless solution is therefore

$$v_0(r) = \frac{1}{r}\frac{\gamma_1^2(\alpha-1)}{1-\eta^2} + r\frac{1-\alpha\eta^2}{1-\eta^2} \tag{8}$$

Due to the inlet conditions, the maximum velocity in the axial direction is $V_0/(\Omega_a b)$ and the mean axial velocity is $\langle w\rangle = 2V_0/(3\Omega_a b)$. The dimensionless equation

$$\langle w\rangle\frac{\partial v}{\partial z} = E\left(\Delta v - \frac{v}{r^2}\right)$$

then becomes:

$$\widetilde{Re}_z\frac{\partial v}{\partial z} = \left(\frac{\partial^2 v}{\partial r^2} + \frac{1}{r}\frac{\partial v}{\partial r} + \frac{\partial^2 v}{\partial z^2} - \frac{v}{r^2}\right) \tag{9}$$

where $\widetilde{Re}_z = Re_z/[3(\gamma_2-\gamma_1)]$. We assume that the azimuthal velocity can be approximated by

$$v(r,z) = v_0(r) + v'(r,z) \tag{10}$$

where the function $v'(r,z)$ takes into account the boundary condition at $z = 0$. This function is expanded in Fourier–Bessel series as follows:

$$v'(r,z) = \sum_{n=1}^{\infty} A_n[Y_1(k_n\gamma_2)J_1(k_n r) - Y_1(k_n r)J_1(k_n\gamma_2)] \times \exp(-\lambda z) \tag{11}$$

where k_n are the positive values of k at which $Y_1(k\gamma_2)J_1(k\gamma_1) - Y_1(k\gamma_1)J_1(k\gamma_2) = 0$, so $k_n \in \{13.9, 26.7, 39.6, \ldots\}$. Substitution of the expression for $v'(r,z)$ in (9) gives the values of the 'half-length' $\lambda(k_n)$:

$$\lambda^2 + \lambda\widetilde{Re}_z - k_n^2 = 0 \Rightarrow \lambda(k_n) = \widetilde{Re}_z\left(\frac{\sqrt{1+4k_n^2\widetilde{Re}_z^{-2}}-1}{2}\right) \tag{12}$$

The term of the series which survives longest corresponds to $n = 1$, and the perturbation due to the inlet boundary condition decays exponentially as $\exp(-\lambda(k_1)z)$, where $k_1 = 13.9$. For large values of the Reynolds number (more precisely for $Re_z \gg 20$), we can estimate the entry length as

$$L_{\text{entry}} = \frac{1}{\lambda(k_1)} \approx \frac{\widetilde{Re}_z}{k_1^2} = \frac{Re_z}{k_1^2}\frac{1}{3(\gamma_2-\gamma_1)} \approx \frac{Re_z}{139} \tag{13}$$

This formula shows that the entry length is proportional to the Reynolds number Re_z but it depends also on the dimensions of the annular channel. So, for given values of the radius ratios, the flow is affected by the inlet perturbation on a larger streamwise distance when increasing Re_z.

The expression (10) also satisfies the inlet boundary condition, namely

$$v(r,0) = r$$

It then follows from (11) that

$$\sum_{n=1}^{\infty} A_n[Y_1(k_n\gamma_2)J_1(k_n r) - Y_1(k_n r)J_1(k_n\gamma_2)] = r - v_0(r) \quad \text{for } \gamma_1 \leqslant r \leqslant \gamma_2$$

whence, following the standard formulae:

$$A_n = \frac{\int_{\gamma_1}^{\gamma_2} x[x - v_0(x)][Y_1(k_n\gamma_2)J_1(k_n x) - Y_1(k_n x)J_1(k_n\gamma_2)]\,\mathrm{d}x}{\int_{\gamma_1}^{\gamma_2} x[Y_1(k_n\gamma_2)J_1(k_n x) - Y_1(k_n x)J_1(k_n\gamma_2)]^2\,\mathrm{d}x}$$

The perturbation of the azimuthal velocity due to the inlet condition can therefore be estimated as

$$v'(r,z) = (r - v_0(r))\exp(-z/L_{\text{entry}}) \quad \text{for } \gamma_1 \leqslant r \leqslant \gamma_2 \text{ and } 0 \leqslant z < +\infty$$

which shows that it depends strongly on the entry length at each point (r,z): the larger the entry length is, the larger the inlet perturbation is. Therefore, the entry length must be sufficiently large so that the noise level induced by the inlet perturbation is sufficient to sustain structures. The above estimation also reveals that, for a fixed value of the Reynolds number, the inlet perturbation increases linearly with the differential rotation rate α (through the expression of $v_0(r)$).

3.2. Propagating Taylor vortices at low values of the Reynolds number

First, flows obtained for small values of the throughflow were examined. The Reynolds number and the Ekman number were fixed respectively to $Re_z = 10$ and $E = 5\times10^{-4}$ (leading to a Rossby number $Ro = 0.022$). The differential rotation rate α was then increased from 1 up to 16.5.

For $\alpha = 14$, the large difference of rotation speed between the flow at inlet and that near the inner cylinder generated a large radial velocity component, involving the attraction of the streamlines by the rotating shaft. The mass transfer took place in this large shear layer on the inner cylinder. This induced the appearance and growth of a large vortex that expanded in the inlet

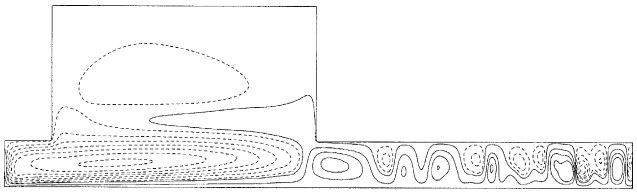

Fig. 2. Streamlines for $E = 5 \times 10^{-4}$, $Re_z = 10$ and $\alpha = 16.5$.

channel and in the channel below the cavity. We can suppose that this vortex, induced by the inlet condition, is an Ekman vortex. Indeed, it is known that, in Taylor–Couette experiments without through-flow, the use of rigid non-rotating end disks to bound the fluid in the axial direction induces stationary Ekman vortices near the end disks. These Ekman vortices were also detected, for small Reynolds numbers, by Tsameret and Steinberg (1994a) in their experiments on open Taylor–Couette systems where meshes at the ends were used as non-rotating boundaries at inlet and outlet. In our case, the flow at inlet has also a zero azimuthal velocity component in the relative frame rotating with the angular velocity Ω_a. The large streamwise expanse of the vortex is probably due to the presence of the side cavity. Besides, an important fluid transfer between the channel and the cavity was observed. The through-flow entered the cavity and was then ejected by the growth of a large toroidal vortex in the cavity. The mass flow transfer between the channel and the cavity decreased with time. In the outlet channel, no TV were observed. At the end of the computation (corresponding to $t \approx 20$), the flow was stationary and its structure was characterized by a large Ekman vortex at inlet, that expanded in the channel down to the downstream part of the cavity.

When the differential rotation rate was increased to $\alpha = 16.5$, the flow structure in the inlet channel and in the cavity was similar. However, TV appeared in the outlet channel and travelled downstream with a velocity equal to $0.86V_0$ (see Fig. 2). In this case, the Taylor number is equal to 15 483, which is larger than the critical Taylor number given by Sparrow et al. (1964) for zero Reynolds number ($Ta_c = 5660$). The reduced Taylor number used by Tsameret and Steinberg (1994b) as relevant parameter is therefore equal to $\varepsilon = (Ta/Ta_c(Re_z = 0) - 1) = 0.8677$ and, according to their phase diagram, the patterns that we observed are PTV in the absolutely unstable regime.

3.3. Effect of the differential rotation rate at large Reynolds numbers

As in the previous cases, the Ekman number was fixed to $E = 5 \times 10^{-4}$. The Reynolds number was increased to $Re_z = 196$. The corresponding Rossby number is $Ro = 0.42$, so the non-linear effects are much more important in this case. The aim was to study instability phenomena occuring for high Reynolds numbers when the differential rotation rate α is increased from 1 to 17.5.

3.3.1. Steady state

For small values of α, the solution was steady. The flow structure in the cavity was characterized by a weak intensity (about 1/16th the main flow intensity) toroidal vortex concentrated near the channel–cavity interface. In the channel, the through-flow was sufficiently strong to prevent the occurence of an Ekman vortex flow near the inlet and, therefore, the streamlines were parallel to the rotation axis (Fig. 3). However, for $\alpha = 8$, the radial profile of the azimuthal velocity in the middle of the inlet channel and its axial profile at $r = 0.096$ (i.e. in the vicinity of the central shaft) revealed the existence of an important shear layer which developed along the inner cylinder. For $Re_z = 196$, formula (13) gives the estimate of the entry length $L_{entry} \approx 1.4$ and the axial profile at $r = 0.096$ of the perturbation v' for the computed solution revealed that, at $z = 1.4$, the perturbation does not represent more than 5.7% of its value at $z = 0$. Therefore, the theoretical estimation (13) fits well with the actual computed entry length.

3.3.2. Convectively and absolutely unstable regimes

After the differential rotation rate was increased from $\alpha = 8$ to 14, a group of small toroidal vortices appeared near the central shaft at the level of the cavity inlet and travelled downstream with time with a phase group velocity about V_0 (Fig. 4(a)). As the group travelled downstream, it also expanded in the axial direction. In the cavity, the flow structure was again characterized by a weak intensity toroidal vortex concentrated near the channel–cavity interface.

The flow disturbances were visualized by substracting the stationary solution obtained for $\alpha = 8$ from the computed one for $\alpha = 14$ (Fig. 4(b)). We then observed in the outlet channel bigger vortices, such as those obtained for $Re_z = 10$ and $\alpha = 16.5$ and therefore very similar to TV, in addition to the small toroidal vortices. These Taylor structures were also clearly visible in the iso-radial velocity patterns. However, according to the instability criteria of Sparrow et al. (1964) for a closed annular channel of radii $a > r_s$ with $r_s/a = 0.25$, the flow for $\alpha = 14$ is always stable whatever the value of the Taylor number. In our case, this means that no TV can

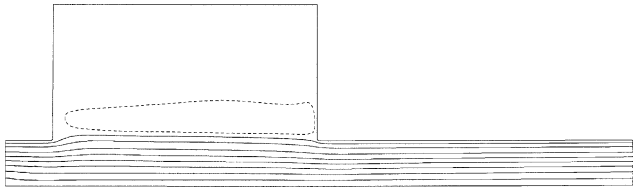

Fig. 3. Streamlines for $E = 5 \times 10^{-4}$, $Re_z = 196$ and $\alpha = 8$.

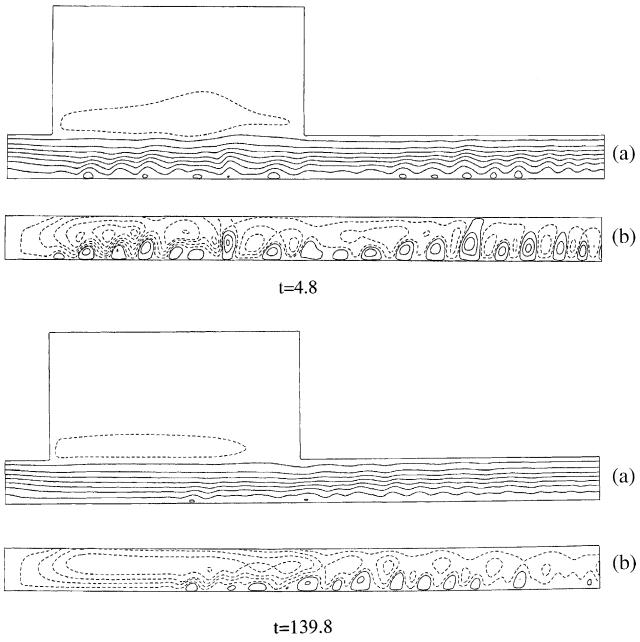

Fig. 4. Instantaneous isovalues of (a) the streamfunction and (b) the perturbations at two dimensionless times ($t = 4.8$ and 139.8) for $E = 5 \times 10^{-4}$, $Re_z = 196$ and $\alpha = 14$.

be observed for $\alpha = 14$, whatever the value of the Ekman number E. Therefore, this suggests that the small toroidal vortices excite a subcritical Taylor instability in the outlet channel. The wave number of this Taylor instability is $k = 6.57$, which is much weaker than that for the small toroidal vortices. Moreover, the results obtained for smaller values of the Reynolds number confirm the fact that this Taylor instability is set-off by the small vortices which are induced by the inlet perturbation. Indeed, for $Re_z = 10$ and $\alpha = 14$, the perturbation generated by the inlet condition is smaller (since the entry length evaluated from (12) is about 0.12, which is 12 times smaller than that for $Re_z = 196$) and, in this case, neither small toroidal vortices nor TV were observed.

In order to characterize the flow regime, we have looked at the evolution with time of the streamfunction in the vicinity of the central shaft at two axial positions: under the upstream part of the cavity (more precisely at $(r_1, z_1) = (0.086, 0.44)$) and under the downstream part of the cavity (more precisely at $(r_2, z_2) = (0.086, 1.4)$) (see Fig. 1). These time histories revealed that the upstream flow becomes stationary (since the small vortices had travelled downstream and had left this part of the channel) whereas the downstream flow exhibits a chaotic behaviour with a frequency peak of about $f \approx 138$. We note that the total computational time $t = 140$ is much larger than the spin-up time, which is about 45.

The fact that the small vortices travelled downstream with time suggests that the flow is convectively unstable as it was observed experimentally by Babcock et al. (1992, 1994) and Tsameret and Steinberg (1994a) in a similar Taylor–Couette configuration (without the side cavity and with only the inner cylinder rotating). However, their study concerns only small values of the forced flow (corresponding to $Re_z < 60$ for Babcock et al. and to $Re_z < 13.5$ for Tsameret and Steinberg). Consequently, although they assume that the flow enters the channel with zero azimuthal velocity (as we do in the relative frame rotating at the angular velocity of the outer cylinder), the noise induced by the inlet condition is much less strong than in our case. Indeed, as it was shown by Tsameret et al. (1994), the intrinsic noise strongly increases with increasing forced flow for large Reynolds numbers. In the same way, the streamwise length in which the flow is affected by the inlet perturbation is much less extended in the system considered by Babcock et al. and by Tsameret and Steinberg. Besides, Babcock et al. evaluated the entry length at about 1.5% of the channel total length L for the Reynolds number considered in the major part of their work, namely $Re_z = 15$. In our configuration, if we assumed that the outlet channel had a finite length $H_s = 32.96$, then the aspect ratio $(H_e + s + H_s)/(a - r_s) = L/(a - r_s)$ would be the same as the one considered in their study and our entry length would represent 4% of the channel length L. Therefore, the inlet perturbation affects the flow on a part of the channel 2.7 times larger than in the case of Babcock et al. We can then suppose that this inlet perturbation is sufficient in our system to sustain the patterns in the convectively unstable regime, whereas Babcock et al. as well as Tsameret and Steinberg had to add an external noise.

The small toroidal vortices also exhibit other characteristics of the PTV in the convectively unstable regime. First, as we noted in the beginning of this section, the wave packet slightly expanded in the axial direction as it travelled downstream, which suggests that the interface separating the pattern state from the base flow fluctuates. Such interface fluctuations were actually observed by Tsameret and Steinberg (1994a) in the case of convective instability. Secondly, the power spectrum of the streamfunction below the downstream part of the cavity exhibits a broad peak, which also characterizes the PTV's power spectrum obtained by these authors in the convectively unstable regime near the outlet of their system.

After the differential rotation rate was increased to $\alpha = 17.5$, the small vortices spreaded inside the whole channel (see Fig. 5), which indicates that the base flow was now absolutely unstable. The vortices continued to travel downstream with a group velocity of about V_0. We observed that, when a vortex travelled downstream, another appeared in its place. So, small vortices were observed in the whole channel for all the computational time, which is $t = 70$, and the interface separating the pattern state from the base flow seemed to be stationary,

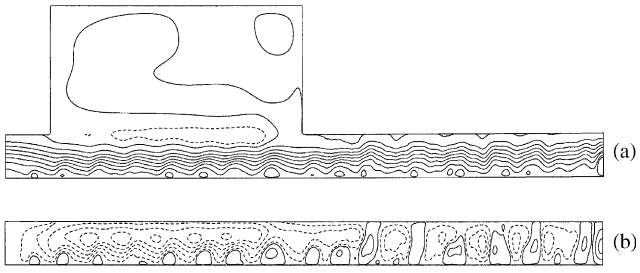

Fig. 5. Instantaneous isovalues of (a) the streamfunction and (b) the perturbations at $t = 75.4$ for $E = 5 \times 10^{-4}$, $Re_z = 196$ and $\alpha = 17.5$.

as it was noted by Tsameret and Steinberg (1994a) in the absolutely unstable region. The disturbed flow, obtained by substracting the stationary solution for $\alpha = 8$ from the numerical solution for $\alpha = 17.5$, revealed bigger TV in the outlet channel. Hence, in the outlet channel, there were once again two types of structures: small toroidal vortices and bigger vortices. If we evaluate the critical Taylor number for $\alpha = 17.5$ by interpolating the critical values given by Sparrow et al. (1964) for $\alpha = 16.7$ and $\alpha = 21.3$, we obtain $Ta_c \approx 5700$. In our case, the value of the Taylor number for $\alpha = 17.5$ is $Ta = 49\,103$ which is therefore much larger than the critical value for the onset of TV. The reduced Taylor number is then $\varepsilon \approx 3.8$. However, this latter information cannot be used to confirm that the flow patterns that we observed are PTV in the absolutely unstable region since the Reynolds number $Re_z = 196$ puts our system largely outside the phase diagram established by Tsameret and Steinberg (1994b).

The analysis of the time history of the streamfunction revealed that the upstream flow is now quasi-periodic with two uncommensurable frequencies $f_1 \approx 167$ and $f_2 \approx 25$. On the other hand, the downstream flow is again chaotic (with a broad frequency peak $f \approx 140$) whereas, according to Tsameret and Steinberg (1994a), the PTV's power spectra in the absolutely unstable regime are noise-free and exhibit sharp frequency peaks (as we observed at the upstream location). It should be noted that the point (r_2, z_2) is located approximatively at the axial position where bigger vortices are revealed by the isovalues of the disturbances (Fig. 5(b)). The noisy power spectrum of the downstream flow could be then associated with a secondary unstable mode. Finally, inside the cavity, the evolution over time of the streamfunction in a point near the channel–cavity interface exhibits also a quasi-periodic behaviour with the same two uncommensurable frequencies $f_1 \approx 167$ and $f_2 \approx 25$.

3.3.3. Transition from absolutely to convectively unstable regime with increasing Reynolds number

Spatial properties: In order to investigate the diagram of stability, the differential rotation rate was fixed to $\alpha = 17.5$ and the Reynolds number was increased from $Re_z = 196$ up to 800.

For $Re_z = 300$, small toroidal vortices appeared near the central shaft in the whole channel at the beginning of the simulation. Then they disappeared in the inlet channel but they were present in the rest of the channel, i.e. below the cavity and in the outlet channel, during all the computational time, $t \approx 40$. Thence, the base flow was still absolutely unstable. The small vortices travelled downstream with a velocity about $0.8V_0$, which is lower than the phase velocity noted for $Re_z = 196$. In the cavity, after a transition time when the channel flow entered the cavity, the flow seemed to become stationary and its structure was similar to the one observed for $Re_z = 196$.

When the Reynolds number was increased to $Re_z = 500$, the small toroidal vortices appeared in almost the whole channel below the cavity and in the outlet channel during all the computational time, $t \approx 60$, which is greater than the spin-up time. Only the part of the channel below the cavity inlet was free of vortices. We can therefore conclude that the base flow was still absolutely unstable. The small vortices moved downstream with time with a velocity about $0.4V_0$, which is half that for $Re_z = 300$. So, the phase velocity of the small vortices decreases when increasing the forced flow, as it can be seen in Fig. 6 presenting the phase velocity as a function of the Reynolds number. In the cavity, the flow structure was the same as that observed for the lower values of the Reynolds number. It should be noted that the results presented above reveal that the distance from the inlet to the interface between the pattern state and the base flow increases with increasing forced flow, as observed by Büchel et al. (1996).

When the forced flow was increased up to $Re_z = 650$, the small toroidal vortices appeared again below the cavity inlet. Then, the wave packet of vortices travelled downstream of the cavity over time, with a velocity about $0.25V_0$, and no more vortices appeared in the channel below the first half of the cavity. This phenomenon is therefore very similar to that observed for $Re_z = 196$ and $\alpha = 14$, which reveals that the base flow was again convectively unstable. When the Reynolds number was increased to $Re_z = 800$, the same phenomenon was observed, and the velocity of the vortices was about $0.22V_0$. So, by increasing the forced flow, the base flow became again convectively unstable. Therefore, the critical value of the differential rotation rate for the onset of convective instability increases with the Reynolds number. This observation is consistent with the stability diagram established by Babcock et al. (1994) and Tsameret and Steinberg (1994a).

Characteristics of the instability: The characteristics of the small toroidal vortices (wave number, frequency in the upstream part of the channel and phase velocity)

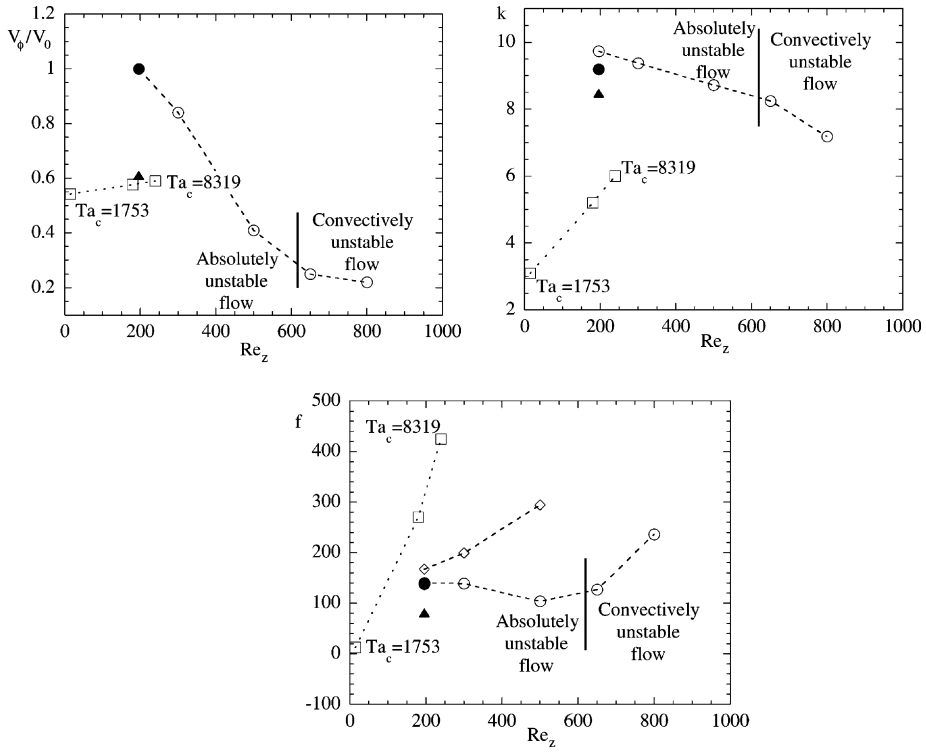

Fig. 6. Variation of phase velocity, wave number and frequency with the Reynolds number: (- -⊖- -) for $Ta = 49, 103$, (•) for $Ta = -53{,}084$, (▲) for $Ta = 12, 276$, (- -⊟- -) for $Ta = Ta_c$ given by Chandrasekhar (1961). The frequency f refers to that of the solution in the channel below the downstream part of the cavity except for $Ta = 49, 103$: (--◇--) in the upstream part and (- -⊖- -) in the downstream part.

for the various cases investigated are reported in Table 2. Their variation with the Reynolds number is also represented in Fig. 6, together with their values at the critical Taylor number given by Chandrasekhar (1961). This figure reveals that the wave number decreases with increasing forced flow and it is always larger than the critical value. The same variation with the Reynolds number has been observed by Tsameret and Steinberg (1994b) for PTV at large Re_z (namely $24 \leqslant Re_z \leqslant 48$). As Büchel et al. (1996), we found a dependence of the wave number on the Taylor number, whereas Tsameret and Steinberg observed only a Re_z dependence. The phase group velocity exhibits the same variation with Ta and Re_z as the wave number. However, it becomes smaller than the critical value for very large Reynolds numbers (namely $Re_z > 500$). Fig. 6 shows also that, for a fixed value of the Taylor number, the phase velocity decreases rapidly with increasing Reynolds number when the base flow is absolutely unstable whereas its decrease is much slower in the case of convective instability. Finally, it can be noted that the frequency peak in the downstream part of the channel exhibits totally different behaviours in the convectively unstable region and in the absolutely unstable one. It decreases slowly with increasing Reynolds number for absolute instability and it increases strongly for convective instability.

3.3.4. Effect of the Ekman number

In order to explore the parameter space, we kept constant again the differential rotation rate $\alpha = 17.5$ and the Reynolds number $Re_z = 196$, and we decreased the rotation parameter Ω_a by increasing the Ekman number from $E = 5 \times 10^{-4}$ to 10^{-3}. In this case, we observed a wave packet of small toroidal vortices travelling downstream with time with a phase velocity about $0.6V_0$. Therefore, the base flow has again become convectively unstable. Moreover, this result shows that the phase velocity varies not only with the forced flow but also with the rotation rate of the channel outer wall.

3.3.5. Effect of the inlet boundary condition

The major part of our results were obtained for a Reynolds number $Re_z = 196$. In this case, the entry length is estimated at about 1.4. Therefore, the flow is affected on a large streamwise distance by the perturbation induced by the inlet boundary condition for azimuthal velocity and, as a consequence (see Section 3.1), this inlet perturbation is sufficiently large to sustain patterns in the convectively unstable regime. Indeed, Tsameret et al. (1994) showed that, for large Reynolds numbers, the most important source of noise is due to inlet perturbations and that this intrinsic noise drastically increases with increasing forced flow.

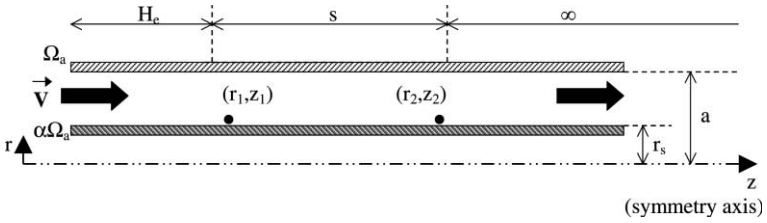

Fig. 7. Taylor–Couette configuration with an axial through-flow.

In order to check the importance of the inlet perturbation for the instability onset, computations were performed using different inlet boundary conditions free of any perturbation. In particular, solution (8) was used as inlet condition for the azimuthal velocity. In this case, no small toroidal vortices were observed near the inner cylinder whatever the values of the Reynolds and Taylor numbers. These results confirm the importance of an inlet perturbation for the onset of small toroidal vortices.

4. Taylor–Couette configuration

The side cavity should be supposed to be a supplementary source of noise in the system. In order to examine the effect of this side cavity on the occurence of small vortices in the channel, we have considered a classical Taylor–Couette configuration (i.e. without the side cavity) but with an axial through-flow (Fig. 7). In this case, the lengths and the velocities are made dimensionless by taking as characteristic length and velocity respectively a and $\Omega_a a$. The Ekman number is defined by $E_{ch} = \nu/(\Omega_a a^2)$ and we have $E_{ch} = 9.7656E$. The radius ratio of the channel is the same as the one considered for the channel–cavity system, i.e. $\eta = r_s/a = 0.25$.

The Reynolds and Ekman numbers were fixed respectively to $Re_z = 196$ and $E_{ch} = 4.88 \times 10^{-3}$ (corresponding to the same angular velocity Ω_a as the one considered for the channel–cavity system for $E = 5 \times 10^{-4}$) and the differential rotation rate α was increased from 1 up to 17.5.

For $\alpha = 14$, a wave packet of small toroidal vortices appeared at $t = 1.9$ near the inner cylinder at a distance about $0.93a$ from the inlet, and travelled downstream over time with a velocity about $0.97V_0$. Therefore, the phase velocity is slightly smaller than that noted in the channel–cavity configuration. In the same way, the wave number is now $k = 10.2$ which is slightly larger than that noted for the previous configuration ($k = 9.19$). At $t = 50.8$, the small vortices only appeared at a distance of about $4a$ from the inlet. Therefore, these small toroidal vortices are induced by a convective instability of the base flow, similar to that observed in the channel–cavity system. The time history of the streamfunction at the same points used in Section 3.3.2 revealed that, in the same way as for the previous configuration, the upstream flow becomes stationary whereas the downstream flow shows a chaotic behaviour. So, the instability phenomenon seems to be very similar to the one observed in the channel–cavity system. The disturbed flow obtained by substracting the stationary solution for $\alpha = 8$ from the solution for $\alpha = 14$ showed that, here again, two types of structures co-existed in the channel: small toroidal vortices and bigger TV (Fig. 8(1)). However, in the present case, the Taylor structures appeared at a distance about $2.9a$ from the inlet at $t = 4.8$ whereas, in the channel–cavity system, they appeared only in the outlet channel i.e. far downstream. So, it seems that the presence of the side cavity prevented the development of the TV in the channel below the cavity and, consequently, these vortices appeared only in the outlet channel.

When the differential rotation rate was increased to $\alpha = 17.5$, the small toroidal vortices spreaded along the whole channel, as in the channel–cavity system, revealing that the base flow was then absolutely unstable (Fig. 8(2)). The small vortices travelled downstream with time with the same velocity than the one for $\alpha = 14$. The time history of the streamfunction showed that the upstream flow is quasi-periodic with two uncommensurable frequencies $f_1 \approx 159$ and $f_2 \approx 29$, which are slightly different from those obtained in the channel–cavity system, whereas the downstream flow is still chaotic.

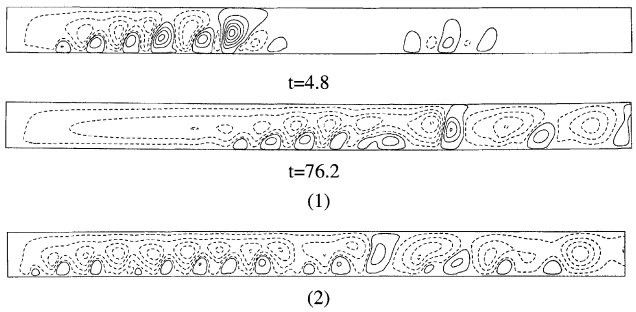

Fig. 8. Taylor–Couette configuration with an axial through-flow. Instantaneous isovalues of the perturbations for $E_{ch} = 4.88 \times 10^{-3}$, $Re_z = 196$ and (1) $\alpha = 14$ (at two dimensionless times $t = 4.8$ and $t = 76.2$); and (2) $\alpha = 17.5$ (at $t = 19.8$).

5. Summary

The purpose of this work was to study the time-dependent flows in a Taylor–Couette-like configuration (with a side cavity) when a strong axial flow is superimposed. A perturbation, due to the mismatch between the rotation of the flow entering the channel and the rotation of the flow inside it, is superposed over the classical base flow. Far from the entry, this perturbation becomes negligible. The entry length, which is the streamwise distance necessary for the flow to recover the azimuthal velocity of the base flow, is found to be proportional to the Reynolds number and depends also on the geometry of the annulus (via the radii of the inner and outer cylinders). The base flow can be convectively or absolutely unstable depending on the values of the Taylor and Reynolds numbers. At low values of Re_z, the absolutely unstable flow shows propagating TV in the outlet channel. At high values of Re_z, the unstable flow is characterized by two patterns: small toroidal vortices which appear at the level of the cavity inlet and then travel downstream over time and bigger vortices which appear only in the outlet channel. When the base flow is absolutely unstable, the small vortices expand also in the upstream direction until the inlet. In the convectively unstable regime, the noise generated by the inlet perturbation is sufficiently strong to sustain the patterns. The results obtained using different inlet boundary conditions suggest that the perturbation induced by the inlet condition for the azimuthal velocity is necessary for the occurence of small toroidal vortices and acts in a similar way as the movements of inlet boundaries used in controlled experiments (Babcock et al., 1992, 1994; Tsameret and Steinberg, 1994a; Tsameret et al., 1994) to trigger the instability.

The results of the computations are presented in Table 2. For small values of the Reynolds number, propagating TV appear in the outlet channel when the Taylor number exceeds the critical value determined by Sparrow et al. (1964) for the same radius ratio (but at zero Reynolds number). For a fixed higher value of the forced flow, and for increasing values of the Taylor number, the base flow becomes first convectively unstable and then absolutely unstable. Further, the critical Taylor number for the onset of convective instability increases with the forced flow. The behaviour of the flow, in terms of stability, is therefore similar to that observed by Babcock et al. (1994) and Tsameret and Steinberg (1994a) in a configuration without a side cavity and with only the inner cylinder rotating. However, two different structures coexist in the outlet channel: small toroidal vortices near the inner cylinder and bigger TV. The small toroidal vortices exhibit several spatiotemporal characteristics of the propagating Taylor vortices, such as the behaviour of the interface between the pattern state and the base flow, in both the convectively and absolutely unstable regimes, or the broadband power spectrum in the convectively unstable regime. On the other hand, their wave number is much larger than those measured in experiments (but for much smaller Reynolds number). When the flow is convectively unstable, the TV appear in the outlet channel for subcritical values of the Taylor number. It seems that the small toroidal vortices near the central shaft trigger a subcritical instability in the outlet channel.

Finally, computations have been carried out in a classical Taylor–Couette configuration in order to identify precisely the role played by the side cavity in the onset of instability. The same dynamical behaviour has been obtained for the same values of the Reynolds and Taylor numbers. This result confirms that, when the base flow is convectively unstable, the noise sustaining the patterns originates essentially from the inlet perturbation.

Acknowledgements

The computations were carried out on the Cray C98 of the C.N.R.S. computing center I.D.R.I.S. The research was made with supports from the "Société de Secours des Amis des Sciences" (Académie des Sciences), from the "Direction Générale de l'Armement" (DRET contract no. 93/150) and from DGESIC Projects BFM2000-0019 and PB98-0074. The authors want to acknowledge gratefully Dr. M. Wilson (University of Bath, UK) and Dr. P. Bontoux (M.S.N.M., Marseille) for their friendly help.

References

Babcock, K.L., Cannell, D.S., Ahlers, G., 1992. Stability and noise in Taylor–Couette flow with throughflow. Physica D 61, 40–60.

Babcock, K.L., Ahlers, G., Cannell, D.S., 1994. Noise amplification in open Taylor–Couette flow. Phys. Rev. E 50 (5), 3670.

Büchel, P., Lücke, M., Roth, D., Schmitz, R., 1996. Pattern selection in the absolutely unstable regime as a nonlinear eigenvalue problem: Taylor vortices in axial flow. Phys. Rev. E 53 (5), 4764–4777.

Chandrasekhar, S., 1961. Hydrodynamic and Hydromagnetic Stability. Oxford, Clarendon Press.

Raspo, I., 1996. Méthodes spectrales et de décomposition de domaine pour les écoulements complexes confinés en rotation, Ph.D. thesis, Université Aix-Marseille II.

Raspo, I., in press. A direct spectral domain decomposition method for the computation of rotating flows in a T-shape geometry. Comput. Fluids.

Raspo, I., Ouazzani, J., Peyret, R., 1996. A spectral multidomain technique for the computation of the Czochralski melt configuration. Int. J. Numer. Meth. Heat Fluid Flow 6, 31–58.

Sparrow, E.M., Munro, W.D., Jonsson, V.K., 1964. Instability of the flow between rotating cylinders: the wide-gap problem. J. Fluid Mech. 20 (part 1), 35–46.

Tsameret, A., Steinberg, V., 1994a. Absolute and convective instabilities and noise-sustained structures in the Couette–Taylor system with an axial flow. Phys. Rev. E 49 (2), 1291–1308.

Tsameret, A., Steinberg, V., 1994b. Competing states in a Couette–Taylor system with an axial flow. Phys. Rev. E. 49 (5), 4077–4086.

Tsameret, A., Goldner, G., Steinberg, V., 1994. Experimental evaluation of the intrinsic noise in the Couette–Taylor system with an axial flow. Phys. Rev. E 49 (2), 1309–1319.

Vanel, J.M., Peyret, R., Bontoux, P., 1986. A pseudospectral solution of vorticity–streamfunction equations using the influence matrix technique. In: Morton, K.W., Baine, M.J. (Eds.), Num. Meth. for Fluid Hydrodynamics II, pp. 463–475.

Werely, S.T., Lueptow, R.M., 1999. Velocity field for Taylor Couette flow with an axial flow. Phys. Fluids 11 (12), 3637–3649.